

# MR Imaging of Intravoxel Incoherent Motions: Application to Diffusion and Perfusion in Neurologic Disorders<sup>1</sup>

Molecular diffusion and microcirculation in the capillary network result in a distribution of phases in a single voxel in the presence of magnetic field gradients. This distribution produces a spin-echo attenuation. The authors have developed a magnetic resonance (MR) method to image such intravoxel incoherent motions (IVIMs) by using appropriate gradient pulses. Images were generated at 0.5 T in a high-resolution, multisection mode. Diffusion coefficients measured on images of water and acetone phantoms were consistent with published values. Images obtained in the neurologic area from healthy subjects and patients were analyzed in terms of an apparent diffusion coefficient (ADC) incorporating the effect of all IVIMs. Differences were found between various normal and pathologic tissues. The ADC of *in vivo* water differed from the diffusion coefficient of pure water. Results were assessed in relation to water compartmentation in biologic tissues (restricted diffusion) and tissue perfusion. Nonuniform slow flow of cerebrospinal fluid appeared as a useful feature on IVIM images. Observation of these motions may significantly extend the diagnostic capabilities of MR imaging.

**Index terms:** Magnetic resonance (MR), physics  
• Nervous system, MR studies

**Radiology** 1986; 161:401-407

<sup>1</sup> From the Groupe de Biophysique, Ecole Polytechnique, 91128 Palaiseau, France (D.L.B.); the Collège d'Evaluation en Résonance Magnétique (CERM), Service de Neuroradiologie, Centre National d'Ophtalmologie des Quinze-Vingts, Paris, (D.L.B., D.L., P.G., E.C., M.L.-J.); and Thomson-CGR, Buc, France (E.B.). Received December 13, 1985; revision requested February 24, 1986; revision received May 15; accepted June 9. Address reprint requests to D.L.B.

© RSNA, 1986

**P**ROTON magnetic resonance (MR) imaging yields contrastive images with excellent spatial resolution and sensitivity. However, the factors of contrast, namely, spin density and apparent T1 and T2 relaxation times, do not allow good characterization of pathologic disorders. Precise MR imaging measurement of these parameters is difficult to perform and subject to artifacts (1). Their *in vivo* significance is unclear. Large differences can be observed among patients with the same pathologic condition; conversely, values obtained in different pathologic conditions may overlap.

Other parameters that can be used for tissue characterization or physiologic information include chemical shift and motions in fluids. The imaging of translational molecular diffusion has been discussed (2-5).

Aspects of molecular diffusion and other incoherent motions that can occur in a voxel, such as microcirculation in capillaries, are reviewed. A description is given of a recently developed MR technique for imaging intravoxel incoherent motions (IVIMs). The diffusion coefficient was measured on phantoms. Normal and pathologic findings in the neurologic area are described and assessed.

## BACKGROUND: MR IMAGING OF DIFFUSION AND OTHER INTRAVOXEL INCOHERENT MOTIONS

### Molecular Translational Self-Diffusion

Molecules in a fluid display a microscopic random translational motion, the so-called Brownian motion. This phenomenon is responsible for molecular diffusion. The mean square of the distance covered is proportional to time and the diffusion coefficient  $D$ , which in turn is a function of the diffusing molecules as well as the solvent's viscosity and tem-

perature. For instance, the diffusion coefficient of water in water (or self-diffusion) at 25°C is  $2.3 \times 10^{-3} \text{ mm}^2/\text{sec}$  (6), and the root mean square distance covered in 100 msec in a given direction is about 20  $\mu\text{m}$ .

### Restricted Diffusion

In the case of some fluids such as intracellular water, diffusion may be restricted to a limited volume. If enough time is allowed for diffusion, the expected free diffusion distance may exceed the available range. When this phenomenon, called "restricted diffusion," occurs, the apparent diffusion coefficient is reduced and becomes a function of the diffusion time and of the geometry of the limiting volume. Many theoretical and experimental studies have addressed the relation between the apparent diffusion coefficient and the shape and size of the restricted volume (7).

### Effect of Diffusion on MR Signal

The detection of diffusion by the spin-echo (SE) technique was described long ago by Hahn (8) and Carr and Purcell (9). The echo signal amplitude  $S$  of the  $n$ th echo is given by

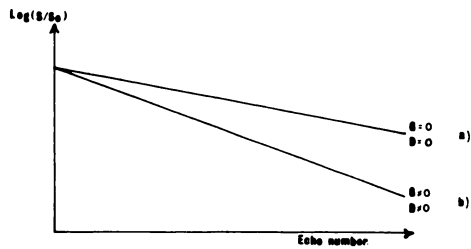
$$S(nTE)/S(0) = \exp[(-n \cdot TE)/T_2], \quad (1)$$

where  $T_2$  is the transverse relaxation time and  $TE$  is the echo delay.

In fact, equation (1) is invalid in the presence of diffusion and a magnetic field gradient. Random displacements of spins caused by molecular diffusion in a magnetic field gradient produce random phase shifts that decrease the echo amplitude (Fig. 1). This attenuation depends on the gradient intensity  $G$ , the diffusion coefficient  $D$ , and the diffusion measurement time. In the case of a constant linear gradient, the diffusion time is  $TE$  and the echo signal is reduced as follows:

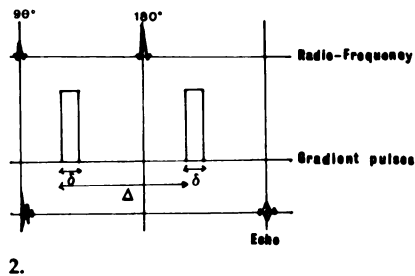
$$S(nTE)/S(0) = \exp[(-n \cdot TE)/T_2] \cdot \exp[(-\gamma^2 \cdot G^2 \cdot D \cdot n \cdot TE^3)/12], \quad (2)$$

where  $\gamma$  is the gyromagnetic factor. Diffusion coefficients can be calculated from



1.

**Figures 1, 2.** (1) Diffusion results in an attenuation of the spin-echo signal  $S$  owing to the random spin motion in the presence of magnetic field gradients. (a) When no gradient or no diffusion is present, the signal decreases owing to T2 relaxation. (b) In the presence of a magnetic field gradient and diffusion, the attenuation is greater. It depends on the gradient strength  $G$ , the diffusion coefficient  $D$ , and the diffusion time (TE in the case of a constant linear gradient). (2) The Stejskal-Tanner sequence (10). Diffusion-related attenuation of the spin-echo signal is obtained by using two intense gradient pulses with a short duration  $\delta$  and separated by a variable time interval  $\Delta$ . As the diffusion time is better defined and the gradient strength can be higher, measurements of diffusion coefficients are more precise.



2.

spin-echo attenuation if the gradient strength  $G$  is known.

Stejskal and Tanner (10) introduced a diffusion measurement method that uses pulsed magnetic field gradients. As gradients are turned off during radio frequency (RF) pulses and during acquisition of the echo signal, a greater gradient strength can be used. This improves the accuracy of the measurement and extends its application to lower diffusion coefficient values. They used a sequence of two intense gradient pulses with a short duration  $\delta$  and separated by a variable time interval  $\Delta$  (Fig. 2). The echo attenuation is then

$$S(nTE)/S(0) = \exp\{-n \cdot TE/T_2\} \cdot \exp\{-\gamma^2 \cdot G^2 \cdot D \cdot \delta^2 \cdot [\Delta - (\delta/3)]\}. \quad (3)$$

### Effect of Other Fluid Motions on MR Signal

Motions, like diffusion, that result in a distribution of phases in a volume element will also produce echo attenuation.

**Tissue perfusion.**—Microcirculation of blood in the capillary network is a motion of this type because there are no preferred orientations as far as sufficient volume element is concerned. It has been described as "macrodiffusion" (11). It can be associated with a pseudo-diffusion coefficient, the value of which is a function of blood velocity and capillary geometry. The pseudo-diffusion coefficient of capillary microcirculation is typically many times greater than the diffusion coefficient of pure water. However, the volume of blood flowing in the perfused capillaries is only a small percentage of the total water content in normal brain tissues.

**Fluid flow.**—The unidirectional, constant linear flow effect on echo signals must be examined separately. It is not an incoherent motion effect but a true non-random flow effect. Use of an SE sequence introduces a flow phase shift on odd-numbered echoes, whereas the refocusing phenomenon occurs only on even echoes (12, 13). The presence in a single

voxel of nonmoving spins and spins moving with several velocities along the direction of the magnetic field gradient will attenuate the echo signal amplitude as a result of a destructive interference phenomenon between various shift phases. This could be the case for a voxel inside a vessel or ventricular cavity in which laminar or turbulent flow results in a distribution of velocities.

### Diffusion in MR Imaging

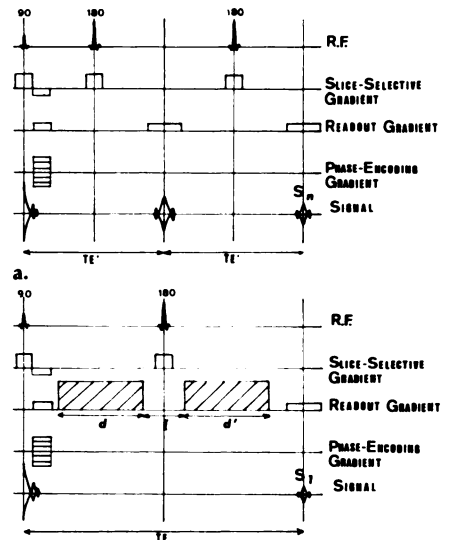
The MR imaging process makes use of three sets of magnetic field gradient pulses for localization of signals (readout, phase-encoding, and section-selective gradients) in the two-dimensional Fourier transform (2DFT) technique. These gradients lead to diffusion-related attenuation if they are large enough. It was pointed out (14) that this attenuation may cause errors in the T2 relaxation time.

On the other hand, Wesbey et al. (2) showed that the effect can be used to image the diffusion coefficients. They could not apply equations (2) and (3) in this report because of the complexity of the series of imaging gradient pulses. Therefore, they determined the diffusion coefficient  $D$  by comparison with the diffusion coefficient  $D_w$  of doped water. The  $D/D_w$  ratio was obtained by comparing the images resulting from different strengths for the section-selective gradient pulses. The method was demonstrated using a phantom thinner than the selected section. One drawback of this method for clinical studies is that the thickness of the imaged section varies with the amplitude of the section-selective gradient.

### METHOD FOR IMAGING INTRAVOXEL INCOHERENT MOTIONS

#### Procedure

To obtain an image in which the contrast depends only on incoherent motions in a voxel, twin SE sequences (3, 4) are used. They differ only in their response



b.

**Figure 3.** IVIM images are calculated by using two sequences. The first (a) is a multi-echo sequence with  $n$  ( $n \geq 1$ ) echoes (here  $n = 2$ ), a short  $TE'$ , and normal gradient pulses. It is insensitive to incoherent motions. The second sequence (b) is a single-echo sequence sensitized to the incoherent motions by a long TE and additional, motion-probing, gradient pulses (duration  $d$  and  $d'$ , separated by a time interval  $l$ ). On a calculated image giving the logarithm of the signal ratio  $S_n/S_1$  for each voxel, the effect of T2 relaxation is eliminated ( $TE = nTE'$ ), as are the effects of spin-density and T1 relaxation ( $TR = TR'$ ). The resulting contrast depends only on intravoxel incoherent motions. Quantitative measurements are obtained on the basis of an apparent diffusion coefficient (ADC) according to equation (6).

to these motions but are identical with regard to the imaging of spin density and T1 and T2 relaxation times (Fig. 3).

The first is a standard 2DFT SE sequence with  $n$  echoes ( $n \geq 1$ ), a  $TE'$  echo delay, and normal gradient pulses. In this conventional sequence, the effect of incoherent motions on the  $n$ th echo signal  $S_n$  is or can be made small (Table 1). The second sequence uses a single-echo sequence. TE is long (typically 120 or 140 msec), and additional gradient pulses, or "motion probing," increase the effect of motions on the echo signal  $S_1$ . The effect of spin density is, of course, the same for both sequences. TE should be equal to  $(n \cdot TE')$ , so that the effect of T2 relaxation is identical for the  $n$ th echo signal  $S_n$  of the first sequence and the signal  $S_1$  of the second sequence. The effect of T1 relaxation is the same for  $S_n$  and  $S_1$  despite the use of different echo trains because repetition time (TR), identical for both sequences, is long enough (TR = 1,000 msec or 1,500 msec) (15).

In the voxel-by-voxel ratio of the two magnitude-reconstructed images, all effects of spin density and T1 and T2 relaxation are eliminated. The intensity in each voxel of the resulting calculated image is a function of intravoxel incoherent

**Table 1**  
Effect of MR Imaging Gradient Pulses on Echo Attenuation: Contribution of Different Gradients to Factor *b* (in sec/mm<sup>2</sup>)

Gradient Axis	Standard Sequence	Sequence with Additional Gradient Pulses	
		G = 0.344 G/cm	G = 0.486 G/cm
Readout gradient	1.14	94.6	179.9
Section-selective gradient	0.02	0.02	0.02
Phase-encoding gradient (maximum value)	1.10	1.10	1.10
Total	2.26	95.7	181.0
S/S(0)*	99.4%	78.7%	63.6%

Note.—Echo signal attenuation owing to diffusion is given by  $S/S(0) = \exp(-b \cdot D)$ . *D* = diffusion coefficient (mm<sup>2</sup>/sec), *b* = gradient factor attenuation (sec/mm<sup>2</sup>). TE is 140 msec. Additional gradient pulses are on the readout gradient axis. Their duration is 40 msec, their intensity *G*, and the time interval between pulses is 28 msec.

\* Attenuation for pure water at 40°C ( $D = 2.5 \times 10^{-3}$  mm<sup>2</sup>/sec).

motions only. In practice, the logarithm of the ratio is displayed, for reasons which will be made clear below.

At the end of the two acquisitions two sets of images are obtained: the conventional spin density, T1- and T2-weighted images currently in use, and the calculated IVIM images of the same sections, displayed using a gray scale.

### Quantitative Determination of the Diffusion Coefficient

In this section, the case in which the motion in the voxel can be characterized as diffusion, with a simple diffusion coefficient *D*, is considered.

To obtain a direct, absolute determination of the diffusion coefficient on images, we must evaluate the effect of all gradient pulses, including both the motion-probing gradients (in the second sequence) and the normal imaging gradients. Starting from Bloch equations, corrected for diffusion effects, the following is found for the attenuation law (3, 4):

$$S(nTE)/S(0) = \exp[(-n \cdot TE)/T2] \cdot \exp(-b \cdot D), \quad (4)$$

where the attenuation factor *b* depends only on the set of gradient pulses.

For a multiecho imaging sequence with *n* echoes using noninterlaced rectangular gradient pulse pairs, *b* is given by

$$b_n = \gamma^2 \cdot \sum_{k=1}^n \sum_{l=x,y,z} G_{kl}^2 \cdot d_{kl}^2 \cdot \{[(d_{kl} + d'_{kl})/3] + I_{kl}\}, \quad (5)$$

where *l* is the axis of the gradient pulses and *k* the interval between echoes.

Each pulse (amplitude *G*, duration *d*) is followed, after a time interval *I*, by a homologous gradient pulse (amplitude *G'*, duration *d'*) with  $G \cdot d = G' \cdot d'$ , such that rephasing of nonmoving spins occurs at each echo. For interlaced pulses, or nonrectangular pulses, equation (5) does not apply, and the attenuation factor *b* is computed numerically.

Background gradients are assumed to be negligible. Changes in the phase-encoding gradient at each cycle complicate the calculation of factor *b*. In practice, it is possible to choose the maximum value for the phase-encoding gradient to be small enough to give negligible effects for motions expected from diffusion (or from perfusion).

Equation (4) is then applied to both the first and second sequence, and the logarithm of the ratio  $S_n/S_1$  is taken. This gives the value of the diffusion coefficient *D* for each voxel according to

$$D(x,y,z) = \{ \ln[S_n(x,y,z)/S_1(x,y,z)] / (b_1 - b_n) \}, \quad (6)$$

in which all quantities, including the factors  $b_n$  and  $b_1$  corresponding to each sequence, are known quantities.

### Assessment of Other Intravoxel Incoherent Motions

The method described above is sensitive to all intravoxel incoherent motions. When such motions are present, the value obtained by applying equation (6) is not a true diffusion coefficient. It is an "apparent diffusion coefficient" (ADC), resulting from all motions. Its value may depend on the motion-probing gradients and on their time interval. It is zero if no motion is present and is equal to the diffusion coefficient *D* if diffusion is the only motion present. It is this sensitivity to other motions that prompts us to use the term "intravoxel incoherent motion imaging" or "IVIM imaging" rather than "diffusion imaging," which has been used previously in a similar context (2-5).

## MATERIALS AND METHODS

IVIM images were obtained with a 0.5-T superconducting, whole-body imager with a head coil (Thomson-CGR, Paris). The normal characteristics were maintained: high-resolution matrix (256 × 256 pixels) and multisection mode. For molec-

ular diffusion, the method was initially evaluated on phantoms. It was then applied in the neurologic area to healthy subjects and to patients.

### Phantom Studies

*D* was measured using a phantom made of a series of 3.5-cm-diameter tubes containing either water or acetone at 25°C. The section thickness was 9 mm, and in-plane spatial resolution was about 1 × 1 mm. The first acquisition used an SE 1,000/140 (TR msec/TE msec) single-echo sequence (*n* = 1). The second acquisition was identical except for the additional or "motion probing" gradient pulses, which were applied on the readout gradient axis. The pulse duration was 40 msec. Two values of gradient intensity were used (0.344 G/cm and 0.486 G/cm) corresponding to 95.7 sec/mm<sup>2</sup> and 181.0 sec/mm<sup>2</sup>, respectively, for factor *b*. Diffusion coefficients were obtained for each tube from calculated images using regions of interest.

### Human Studies

MR images of intravoxel incoherent motions were obtained from healthy subjects and from patients with neurologic disorders. Normal brain tissues and brain tumors (one low-grade astrocytoma, one cystic astrocytoma with an obstructive hydrocephalus, and two brain metastases) were studied for the preliminary work. Diagnosis had previously been established by other methods, including computed tomography (CT), standard MR imaging, and in some cases, surgery.

A set of three sections was obtained for both acquisitions. The position and orientation of the sections were chosen according to expected pathologic conditions and/or standard acquisitions. The section thickness was 9 mm with a 9-mm inter-section gap. The in-plane spatial resolution was 1.09 × 1.09 mm (28 × 28-cm field of view, 256 × 256-pixel matrix). The conventional first acquisition was either an SE 1,500/60, 120 double-echo sequence, or an SE 1,500/120 single-echo sequence in the case of quantitative measurements. The second sequence, sensitized to intravoxel incoherent motions, was an SE 1,500/120 single-echo sequence with additional gradient pulses on the readout axis. A TR of 1 second was sometimes used to reduce the imaging time.

At the end of the two acquisitions, the standard images were displayed with the calculated IVIM images. Images were assessed qualitatively, and regions of interest were defined for quantitative measurements of the ADC.

## RESULTS

### Phantom Diffusion Studies

The only intravoxel incoherent motion expected was diffusion, since care was taken to avoid thermal con-

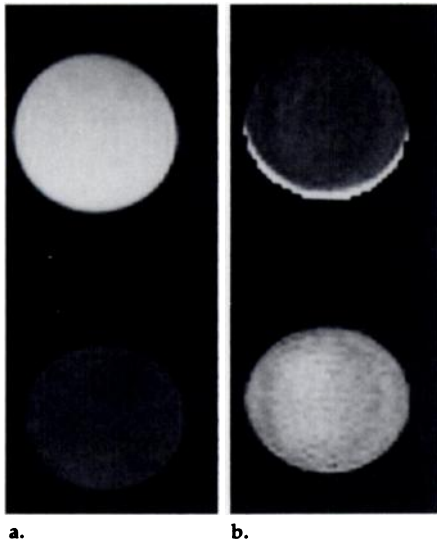


**Figure 4.** Images of a phantom made of tubes containing water (top) and acetone (bottom) at 25°C. The section thickness is 9 mm, and the in-plane resolution 1 × 1 mm. (a) Standard sequence (SE 1,000/140). Signal in water is higher than in acetone owing to the respective T1 and T2 relaxation times. (b) Calculated diffusion image. The contrast in this image is inverted in relation to a, showing that diffusion in acetone is greater than in water. Note the shiftlike artifact beside the water tube owing to residual gradients produced by eddy currents during data sampling in the second sequence.

vection. Phantom diffusion images are shown in Figure 4. Diffusion in acetone appeared to be greater than in water. The diffusion coefficients computed from images, given in Table 2, agreed with published values (2, 6, 16, 17). Two values of the gradient were used, corresponding to  $b = 95.7$  and  $181.0 \text{ sec/mm}^2$ . They led to the same results. Different coefficients obtained from several acquisitions were the same within 5%.

### Human Studies

The results were analyzed in terms of an ADC, which incorporates the effect of all possible intravoxel incoherent motions.

### Normal Tissues

In images of the normal head (Fig. 5), gray matter had a higher ADC than white matter did (about  $2.0 \times 10^{-3} \text{ mm}^2/\text{sec} \pm 0.1 \times 10^{-3}$  and  $1.7 \times 10^{-3} \text{ mm}^2/\text{sec} \pm 0.1 \times 10^{-3}$ , respectively). The ADC of cerebrospinal fluid (CSF) varied according to the location. It was the same as the diffusion coefficient of pure water (about  $2.5 \times 10^{-3} \text{ mm}^2/\text{sec} \pm 0.2 \times 10^{-3}$  at 40°C) in the horns of the lateral ventricles but was significantly higher in the third and fourth ventricles.

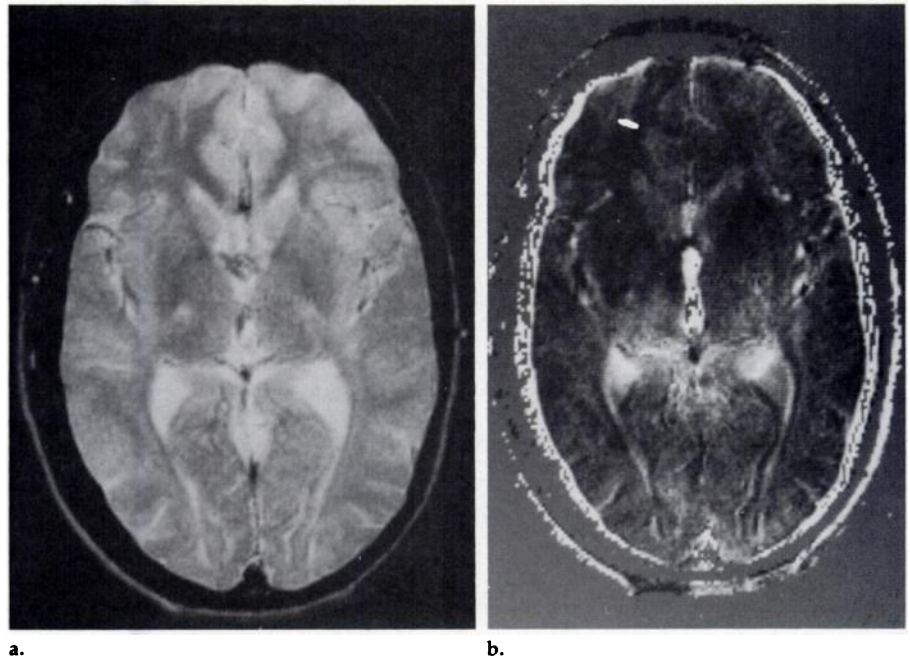


**Figure 5.** Normal head (transverse images). (a) Standard sequence (SE 1,000/140). (b) IVIM image. The apparent diffusion coefficient (ADC) in gray matter is higher than in white matter. This may be related to a differential perfusion effect. The ADC of CSF in ventricular cavities is heterogeneous. An ADC higher than the diffusion coefficient of pure water is observed in various locations because of CSF flow (third ventricle).

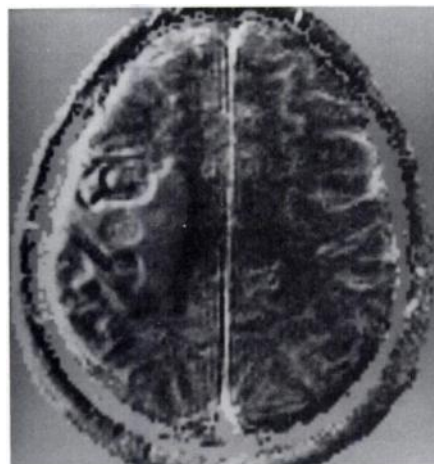


**Figure 6.** Brain metastasis with edema (transverse image). IVIM image. The ADC in the metastasis is heterogeneous and in places higher than the diffusion coefficient of pure water. This is related to enhanced internal perfusion. The edema around the tumor appears homogeneous with sharply defined border and with an ADC slightly greater than that of normal brain tissue.

### Pathologic Cases

Qualitative differences were observed between various tumors. A large ADC ( $>3.5 \times 10^{-3} \text{ mm}^2/\text{sec}$ ) was found in places in a brain metastasis (Fig. 6). A very homogeneous area of slightly elevated ADC with well-defined boundaries was observed around the tumor. It occupied

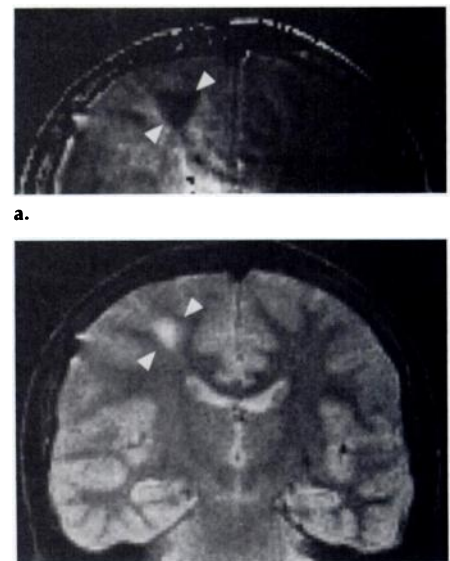


**Figure 7.** Low-grade astrocytoma (arrowheads) (frontal images). (a) IVIM image. The ADC in the tumor is very low, probably because of restricted diffusion in this small cell tumor and poor perfusion. (b) Standard sequence (SE 1,500/120).

the location assigned to edema on CT and MR images. The value for a low-grade astrocytoma (Fig. 7) was very small ( $<1.5 \times 10^{-3} \text{ mm}^2/\text{sec}$ ). The ADC of a cystic lesion (astrocytoma) with hydrocephalus (Fig. 8) was equal to the diffusion coefficient of

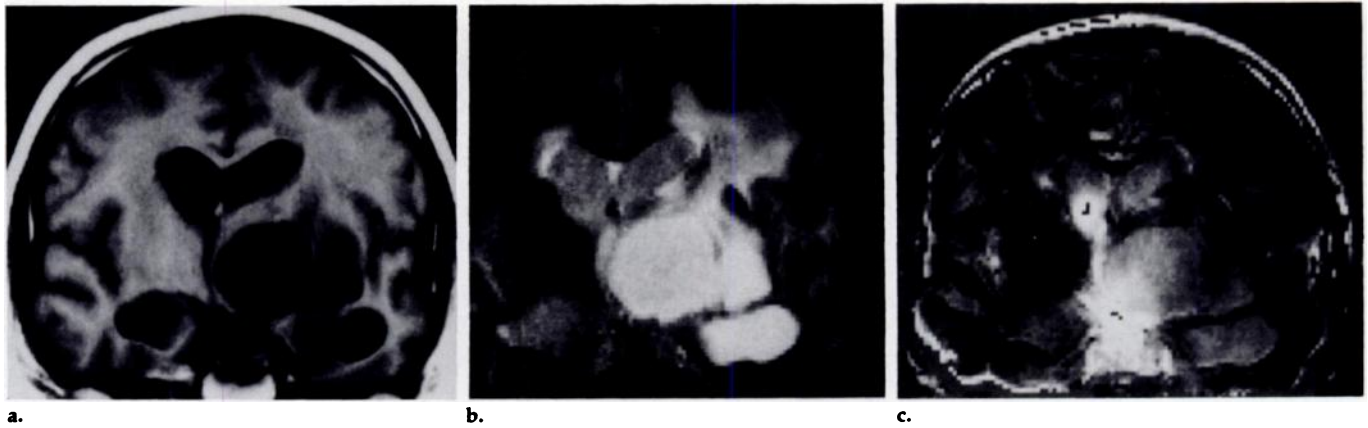


**Figure 8.** Cystic astrocytoma with hydrocephalus (frontal images). (a, b) Standard spin-echo images (a, SE 400/28; b, SE 1,500/120). (c) IVIM image of the same section. The ADC in the lesion is high, similar to that of CSF in anterior horns of the lateral ventricles, which is compatible with its cystic nature (free diffusion vs. restricted diffusion in normal brain tissues). Note the area with very high signal intensity in the dilated ventricular cavities, starting from the right foramen of Monro and going through the third ventricle; the high signal intensity is due to the moving CSF. No flow effect is seen in the left foramen of Monro.

**Table 2**  
Diffusion Coefficients of Phantom ( $\times 10^{-3}$  mm<sup>2</sup>/sec at 25°C)

Fluid	Measured with $b_n - b_1 = 93.4$ sec/mm <sup>2</sup>	Measured with $b_n - b_1 = 178.7$ sec/mm <sup>2</sup>	Literature Values
Water	2.35 $\pm$ 0.10	2.40 $\pm$ 0.10	2.25–2.51 (6)
Acetone	4.47 $\pm$ 0.22	4.49 $\pm$ 0.22	4.5–4.8 (16, 17)

Note.—Diffusion coefficients were imaged and then computed from the images in a region of interest.

water, as observed also for CSF in the dilated anterior horns of the lateral ventricles. On the other hand, the ADC in the third ventricle was high, and the ADC of the right foramen of Monro, opposite the lesion, was much higher than the ADC of the left foramen.

## DISCUSSION

### Imaging Method

**Confirmation.**—The method described here makes it possible to obtain in vivo images of intravoxel incoherent motions, such as diffusion or microcirculation. These motions are characterized in calculated images by an ADC, which can be quantitatively measured. The ADC obtained in vitro for water and acetone agreed with published values of the diffusion coefficients of these media (2, 6, 16, 17). In particular, ADC values were independent of the magnetic field gradient pulses used for their measurement. These results support the theoretical analysis. Other studies with pertinent phantoms are in progress to evaluate the contribution of the other intravoxel motions, especially microcirculation, to the ADC.

**Limitations.**—When quantitative measurements are desired, care must be taken to avoid possible systematic errors, particularly in clinical studies.

1. Use of a multiecho sequence for the first sequence allows physicians to obtain various T2-weighted images for clinical assessments; we followed this procedure in our early experiments. Unfortunately, multiecho sequences are prone to many potential artifacts (1, 18). Errors in selective RF pulse flip angles, particularly in the 180° pulses, can reduce the amplitude of the last echoes. They generate stimulated echoes (8). To avoid such artifacts, a single-echo sequence should be used for the first sequence to obtain quantitative measurements. A multiecho sequence is appropriate only for qualitative evaluations.

2. Use of long echo delay times (more than 100 msec) requires long T2 relaxation times, a situation found for both normal and pathologic tissues in the neurologic area. When T2 values are shorter, as is possible in other organs, the signal-to-noise ratio (S/N) at long echo times could become too low. In this case, consideration might be given to a method based on stimulated echoes (5, 19), if T1 is much longer than T2. The use-

fulness of this procedure in imaging is yet to be demonstrated.

3. The strong gradient pulses (about 0.35 G/cm) used in our experiments may produce eddy currents in the MR imaging unit. Residual magnetic field gradients will result. Their contribution to the diffusion effect is found to be quite small; however, they create significant gradients during the data acquisition period.

When the original gradient pulses are in the direction of the readout gradient, the image is dilated (or contracted) in this direction. This artifact affects only the second image, since no extra gradient is applied in the first one. When they are combined to yield the intravoxel motion image, a shiftlike artifact can be seen that becomes more pronounced the farther it is from the center (Fig 4b). Such artifacts can be compensated for by appropriate shaping of the current pulses sent into the gradient coils. Additional data processing correction may be carried out on the basis of the previously recorded changes in image size when the additional gradient pulses are switched on and off.

4. The only fluid motions detected are those in the direction of the additional gradient, that is, along the readout axis. For isotropic motions, this is inconsequential. In other cases, the motion along various directions can be explored by exchanging the direction of the readout and phase-encoding gradients. An alternative possibility would be to generate additional gradient pulses along the direction of the phase-encoding gradient.

## Biologic Content of IVIM Images

The ADC of water measured in biologic tissues with this method is different from the diffusion coefficient of water in vitro. Furthermore, it shows large variations between normal and pathologic tissues.

Signal intensity in calculated images may be due to various intravoxel motions: diffusion (or restricted diffusion), perfusion, or nonuniform flow. Work in progress is aimed at systematically distinguishing between these various sources. For the time being, the signals must be assigned in an ad hoc manner; but they may, nevertheless, be useful for tissue characterization.

## Diffusion and Restricted Diffusion

The diffusion coefficient of water in biologic tissues is recognized as being about half that of pure water (20–22). However, compartmentation in biologic tissues can further reduce the measured diffusion coefficient, in relation to a restricted diffusion phenomenon, and could explain some of the very low diffusion coefficients observed. During the diffusion measurement time (about 110 msec in our experiments), the range of nonrestricted diffusion of water in a biologic tissue would be about 15  $\mu\text{m}$ . Assuming that the mean size of cells is smaller than this free diffusion range, a restricted diffusion effect occurs and reduces the measured diffusion coefficient. In several studies of biologic systems, the restricted diffusion coefficients of water have been related to cell size and to the presence of intracellular structures (21, 22). The effect of restricted diffusion could be minimized by using shorter diffusion measurement times. However, this raises practical difficulties since the gradients would have to be stronger. On the other hand, one could also try to increase the effect of restricted diffusion by increasing the diffusion measurement time. S/N might then become too small for a long echo delay in relation to T2 relaxation times in biologic tissues. Use of stimulated echoes might be an alternative solution.

## Tissue Perfusion

In some cases, the ADC is large, sometimes even larger than  $D_w$ , the diffusion coefficient of pure water. This is a specific characteristic of living tissues and is related to tissue

perfusion. The ADC resulting only from microcirculation can be many times greater than  $D_w$  owing to the velocity of blood water in capillaries, which is in the range of 1–4 mm/sec (23). However, only a small percentage of all the water present in a voxel is concerned. The resulting ADC measured with our method is a function of the diffusion coefficient (which can be a restricted diffusion coefficient) of the static component in the tissue and of a term depending on the fractional volume  $f$  of active capillaries, that is, capillaries in which blood circulates.

## CSF Flow

The ADC measured in those ventricular cavities in which the CSF is known to flow faster, particularly in narrow areas such as in the third ventricle and in the foramina of Monro, was much higher than the diffusion coefficient of water. This can be explained by a nonuniform flow effect according to the existence in a single voxel of several velocities, as stated above. Despite the relatively slow rate of CSF flow, this effect can be made significant by using a single-echo mode with additional gradient pulses in the second sequence. CSF flow resulting in echo attenuation was seen to be useful in IVIM images even though it is not an incoherent motion. It was generally easy to distinguish from diffusion or perfusion by its high intensity and its topography. Another assignment method would be to eliminate the effect of constant linear flow when using flow-compensated bipolar gradient pulses (24), which result in a zero phase shift for both odd and even echoes.

These considerations will now be applied to the discussion of a few clinical cases.

## Clinical Applications

*Gray and white matter (Fig. 5).*—The ADC in these tissues was less than the diffusion coefficient of pure water. However, it was higher than that observed in ex vivo biologic tissues (20–22). These differences may be partly related to a perfusion effect, factor  $f$  being about 5% and 2% for gray and white matter, respectively (25).

*Metastasis and edema (Fig. 6).*—The ADC was heterogeneous and higher than the diffusion coefficient of water in some places, suggesting enhanced perfusion in this tissue. The

ADC in the surrounding edema was slightly higher than in the corresponding tissue and was almost as high as that of free water.

*Low-grade astrocytoma (Fig. 7).*—The ADC in this tumor was lower than in normal brain tissue. This finding implies that the volume of perfusing fluid was not very great and that diffusion was probably restricted by the small size of the cells.

*Cystic astrocytoma and hydrocephalus (Fig. 8).*—The high ADC of the tumoral tissue, similar to that observed in the anterior horns of the lateral ventricles, was probably due to its cystic nature, which allows free (nonrestricted) diffusion. The ADC of the CSF was particularly high inside both the right foramen of Monro and the third ventricle. This must have been due to nonuniform CSF flow, which was thus visualized in a direct fashion. The left foramen of Monro did not have such a high ADC, suggesting obstruction. This was confirmed surgically.

The imaging method for intravoxel incoherent motions that has been presented here may potentially be used in the quantitative and separate evaluation of diffusion, restricted diffusion, perfusion, and nonuniform slow flow, without using contrast agents. Although more work is needed to reach these objectives fully, the examples given here show that IVIM imaging can significantly improve the capability of MR imaging for tissue characterization and functional studies. ■

**Acknowledgment:** The authors thank Professor Maurice Guéron for his invaluable assistance in the preparation of the manuscript.

## References

1. Young IR. Artifacts in the measurement of T1 and T2. In: Abstracts of the 4th annual meeting of the Society of Magnetic Resonance in Medicine. Berkeley, Calif.: Society of Magnetic Resonance in Medicine, 1985; 16–17.
2. Wesbey GE, Moseley ME, Ehman RL. Translational molecular self-diffusion in magnetic resonance imaging: effects and applications. In: James TL, Margulis AR, eds. Biomedical magnetic resonance. San Francisco: Radiology Research and Education Foundation, 1984; 63–78.
3. Le Bihan D, Breton E, Syrota A. In-vivo self-diffusion magnetic resonance imaging. In: Abstracts of the 4th annual meeting of the Society of Magnetic Resonance in Medicine. Berkeley, Calif.: Society of Magnetic Resonance in Medicine, 1985; 1238–1239.
4. Le Bihan D, Breton E. Imagerie de diffusion in vivo par résonance magnétique. CR Acad Sci Paris 1985; 301 série II, 15:1109–1112.
5. Merboldt KD, Hanicke W, Frahm J. Self-diffusion NMR imaging using stimulated

- echoes. *J Magn Reson* 1985; 64:479-486.
6. James TL, McDonald GG. Measurement of the self-diffusion coefficient of each component in a complex system using pulsed-gradient Fourier transform NMR. *J Magn Reson* 1973; 11:58-61.
  7. Tanner JE, Stejskal EO. Restricted self-diffusion of protons in colloidal systems by pulsed-gradient, spin-echo method. *J Chem Phys* 1968; 49:1768-1777.
  8. Hahn EL. Spin echoes. *Phys Rev* 1950; 80:580-594.
  9. Carr HY, Purcell EM. Effects of diffusion on free precession in nuclear magnetic resonance experiments. *Phys Rev* 1954; 94:630-635.
  10. Stejskal EO, Tanner JE. Spin diffusion measurements: spin-echoes in the presence of a time-dependent field gradient. *J Chem Phys* 1965; 42:288-292.
  11. Budinger TF, Knittel BL, Bruner P, Harrison C. Tissue perfusion phantom for magnetic resonance flow studies. In: Abstracts of the 4th annual meeting of the Society of Magnetic Resonance in Medicine. Berkely, Calif.: Society of Magnetic Resonance in Medicine, 1985; 577-588.
  12. Waluch V, Bradley WG. NMR even echo rephasing in slow laminar flow. *J Comput Assist Tomogr* 1984; 8:594-598.
  13. Von Schulthess GK, Higgins CB. Blood flow imaging with MR: spin-phase phenomena. *Radiology* 1985; 157:687-695.
  14. Wesbey G, Moon K, Crooks L, Arakawa M, Brasch R. Proton T2 reduction due to spin-diffusion through pulsed gradients in spin-echo NMR imaging: imaging implications and applications. In: Abstracts of the 2d annual meeting of the Society of Magnetic Resonance in Medicine. Berkeley, Calif.: Society of Magnetic Resonance in Medicine, 1983; 375-376.
  15. Max LS. Measurement of spin-lattice relaxation times in double spin-echo imaging. *J Magn Reson Med* 1984; 1:361-369.
  16. McCall DW, Douglass DC, Anderson EW. Diffusion in liquids. *J Chem Phys* 1959; 31:1555-1557.
  17. Cantor DM, Jonas J. Automated measurement of self-diffusion coefficients by the spin-echo method. *J Magn Reson* 1977; 28:157-162.
  18. Majumdar S, Gore JC, Orphandoudakis SC. Errors in estimations of T2 from multiecho sequences using selective excitation: implications for MR imaging. In: Abstracts of the 4th annual meeting of the Society of Magnetic Resonance in Medicine. Berkely, Calif.: Society of Magnetic Resonance in Medicine, 1985; 79-80.
  19. Tanner JE. Use of stimulated echoes in NMR diffusion studies. *J Chem Phys* 1970; 52:2523-2526.
  20. Tanner JE. Self-diffusion of water in frog muscle. *Biophysiol J* 1979; 28:107-116.
  21. Cooper LC, Chang DB, Young AC, Martin CJ, Johnson B. Restricted diffusion in biophysical systems. *Biophysiol J* 1974; 14:161-177.
  22. Cleveland GG, Chang DC, Hazlewood CF, Rorschach HV. Nuclear magnetic resonance measurement of skeletal muscle: anisotropy of the diffusion coefficient of the intracellular water. *Biophysiol J* 1976; 16:1043-1053.
  23. Lee J. Pressure-flow relationships of single vessels and organs. In: Gabor K, Burton MA, eds. *Microcirculation*. Baltimore: University Park, 1977; 335-364.
  24. Le Roux P, Floch J. Cancellation of the shear rate influence on flow velocity imaging. In: Abstracts of the 4th annual meeting of the Society of Magnetic Resonance in Medicine. Berkely, Calif.: Society of Magnetic Resonance in Medicine, 1985; 585-586.
  25. Weiss HR, Buchweitz E, Murtha TJ, Auletta M. Quantitative regional determination of morphometric indices of the total and perfused capillary network in the rat brain. *Circ Res* 1982; 51:494-503.